

# UC Davis

## UC Davis Previously Published Works

### Title

First principles modelling of the ion binding capacity of finger millet.

### Permalink

<https://escholarship.org/uc/item/8dd0v5nk>

### Journal

npj Science of Food, 8(1)

### Authors

Yong, Wei

Lin, Tsair-Fuh

Chappell, Helen

et al.

### Publication Date

2024-05-14

### DOI

10.1038/s41538-024-00270-1

Peer reviewed



# First principles modelling of the ion binding capacity of finger millet



Wei Cong Matthew Yong<sup>1</sup>, Apramita Devi<sup>2,3</sup>, Tsair-Fuh Lin<sup>3</sup> & Helen F. Chappell<sup>1</sup> ✉

Finger millet, a cereal grain widely consumed in India and Africa, has gained more attention in recent years due to its high dietary fibre (arabinoxylan) and trace mineral content, and its climate resilience. The aim of this study was to understand the interactions between potassium ( $K^+$ ), calcium ( $Ca^{2+}$ ) and zinc ( $Zn^{2+}$ ) ions and the arabinoxylan structure and determine its ion-binding capacity. Three variations of a proposed model of the arabinoxylan structure were constructed and first principles Density Functional Theory calculations were carried out to determine the cation-binding capacity of the arabinoxylan complexes.  $Zn^{2+}$ -arabinoxylan complexes were highly unstable and thermodynamically unfavourable in all three models.  $Ca^{2+}$  and  $K^+$  ions, however, form thermodynamically stable complexes, particularly involving two glucuronic acid residues as a binding pocket. Glucuronic acid residues are found to play a key role in stabilising the cation-arabinoxylan complex, and steric effects are more important to the stability than charge density. Our results highlight the most important structural features of the millet fibre regarding ion-storage capacity, and provide valuable preliminary data for confirmatory experimental studies and for the planning of clinical trials where the bioavailability of bound ions following digestion may be tested.

Mineral deficiencies (e.g. iron, calcium and zinc) are some of the leading nutritional problems worldwide, affecting human physical and mental development across the spectrum of high, middle and low-income countries<sup>1,2</sup>. While food fortification and mineral supplementation are globally accepted interventions to combat these deficiencies<sup>3</sup>, the lack of trace mineral bioavailability in some of these mineral-enriched foods remains a significant concern. Nutrients such as dietary fibre, polyphenols, phytic acid, and proteins, which are intrinsic nutritional components, have all been reported to bind with mineral ions, sometimes reducing the ion bioavailability<sup>4,5</sup>.

Millets are a 'superfood' at the forefront of mineral fortification initiatives in developing countries, especially in Asia and Africa, where this grain is often the major staple food for large sections of the population<sup>6</sup>. Indeed, the United Nations General Assembly declared 2023 to be the International Year of Millets, to promote awareness of the vital importance of this crop to millions of people. Worldwide millet production has reached ~33.6 million tonnes per year, of which India accounts for 35.3% of the total<sup>7</sup>. Millets are a drought-resilient crop<sup>8</sup> genetically adapted to suit hot, dry climates<sup>9</sup>, with high levels of macronutrients (dietary fibre and protein) and minerals (iron, calcium and zinc). The most important species of commercially produced millet are pearl (*Cenchrus americanus* (L.)

Morrone; *Pennisetum glaucum*), finger (*Eleusine coracana*), foxtail (*Setaria italica*), and proso (*Panicum miliaceum*). There is, in addition, a number of other more minor millet species which are often cultivated in specific geographic areas, for example, Kodo (*Paspalum scrobiculatum* (L.)), Little (*Panicum sumatrense*) and Barnyard (*Echinochloa esculenta* A.)<sup>10</sup>. Notably, each millet species is rich in a particular mineral; for example, pearl millet is rich in iron, finger millet in calcium and foxtail millet in zinc<sup>6,11</sup>.

An important concern in using millet as the solution to mineral deficiency in low and middle-income countries, through biofortification or supplementation, is the high antinutritional factors (ANFs) such as phytates, tannins, oxalates and dietary fibre (DF) content. To date, phytate is the most studied antinutritional factor studied for millets, with limited focus on other ANFs<sup>12</sup>. Millets are reported to be high in a mixture of carbohydrate polymers such as arabinoxylans, hemicelluloses and glucans<sup>13–16</sup>, and it has long been a concern that such dietary fibres play a potentially detrimental role in trace mineral bioavailability<sup>4</sup>. However, the chemistry of mineral-fibre complexation is still ambiguous. It remains unclear whether this effect on mineral bioavailability is valid equally for all types of dietary fibres<sup>4,5</sup>.

A limited amount of work has been undertaken on the structural characterisation of the arabinoxylans, glucans and celluloses in millets<sup>14,15,17–22</sup>. However, in cereal grains such as millets, the main type of

<sup>1</sup>School of Food Science and Nutrition, University of Leeds, Leeds, UK. <sup>2</sup>Department of Viticulture and Enology, University of California, Davis, CA, USA.

<sup>3</sup>Department of Environmental Engineering, National Cheng Kung University, Tainan, Taiwan. ✉e-mail: [H.F.Chappell@leeds.ac.uk](mailto:H.F.Chappell@leeds.ac.uk)

hemicelluloses (dietary fibres) are arabinoxylans, which are predominantly found in the bran layer<sup>23</sup>. For example, analysis of foxtail millet found that the bran consisted of 79.22% dietary fibres, of which 47.83% was the insoluble hemicellulose, itself composed of 88.89% arabinose and xylose<sup>23</sup>. More specifically, for finger millet, spectroscopic studies using carbon and proton nuclear magnetic resonance (<sup>13</sup>C NMR, <sup>1</sup>H NMR) and Fourier transform infrared spectroscopy (FTIR) revealed that the structure was made up of a β-D (1,4)-linked xylan backbone, with branching on the main chain predominantly made up of arabinose residues and uronic acid residues<sup>18</sup>. Similarly, Nandini and Salimath<sup>15</sup> found that the uronic acid content in pearl millet was about 6%, and these uronic acid residues were substituted across the xylan backbone chain. Only one study has explicitly examined ion binding, using simple supplementation experiments on sorghum and finger millet<sup>24</sup>. That work indicated that nutritionally significant minerals (iron, calcium and zinc) vary in their affinity for the bulk dietary fibres, with calcium being the most likely to bind.

A small number of studies have focused on the influence of dietary fibre on the mineral bioavailability in millets using in vitro estimations only<sup>25,26</sup>. Amalraj and Pius<sup>25</sup>, examining both pearl and finger millet, found that the bioavailable percentage of calcium, determined through a synthetic-digestion process, was marginally lower in finger millet (28% raw; 28.6% cooked) than pearl millet (29.8% raw; 30.3% cooked) and wheat (34.9% raw; 34.8% cooked), even though the total calcium, determined by atomic adsorption spectroscopy, was more than seven times higher than pearl millet, and six times higher than wheat. This lower calcium bioavailability corresponds to a higher DF content of finger millet compared to other cereals.

Lestienne et al.<sup>26</sup> found that fibres and tannins play an important role in reducing in vitro iron and zinc bioavailability for pearl millet by chelating the high proportion of the mineral in grain hulls. However, none of the studies evaluated the role or chemistry of specific structural components of dietary fibre on mineral binding and bioavailability. Additionally, it must be remembered that in vivo, although humans are unable to breakdown the arabinoxylan structures found in millet, gut microbiota (particularly in the colon) produce a vast array of xylanolytic enzymes capable of both degrading the xylan backbone, and cleaving the side-chain residues<sup>27,28</sup>. This suggests that ion-binding within the arabinoxylan structures is likely to be a positive element of this crop's nutrient-delivering capacity and highlights the difficulty in assessing bioavailability in vitro.

Employing state-of-the-art first-principles computational modelling software, such as the Cambridge Serial Total Energy Package (CASTEP)<sup>29</sup> Density Functional Theory (DFT) code, is a particularly effective way of probing the structure and chemistry of molecular systems, providing the atomistic and molecular detail that is missed in experimental studies. DFT has been used previously to study the interaction of a variety of mono and divalent cations with other polysaccharides such as algal and bacterial alginates, chitosan, and pectin<sup>30–34</sup>. These studies have demonstrated that metal cations can form complexes with other polysaccharides in which the hydroxyl and carboxylic acid functional groups of the saccharide structures play a vital role in the cation binding. However, to date, no studies have demonstrated the interaction chemistry between essential trace metals and the arabinoxylan structure of millets.

For this computational study, aimed at identifying the structural elements of the arabinoxylan chains that are responsible for ion-retention, finger millet was chosen. Finger millet is generating considerable research interest with respect to eliminating calcium deficiency in the poorest regions<sup>35</sup> as it contains the highest levels of calcium of all the millets (and of most other grains) at 364 mg/100 g, as well as high potassium (443 mg/100 g) and zinc (2.5 mg/100 g) levels<sup>6</sup>. To date, the only two studies that assessed calcium retention from finger millet in humans<sup>36,37</sup> showed calcium retention levels between 19.7 and 26%. While promising, it should be noted that each study only included eight participants, resulting in a lack of statistical power<sup>38</sup>. However, statistical analysis<sup>38</sup> of four in vitro studies<sup>39–42</sup> on the bioavailability of calcium from finger millet when processed by different methods, highlighted the potential of finger millet as a bioavailable source of

calcium, with an average bioavailability of 44.1 ± 14.5% in raw or unprocessed grains, and 61.4 ± 21.5% in processed millet<sup>38</sup>. Interestingly, not all methods of processing resulted in increased bioavailability (e.g. expansion and popping reduced the bioavailability by close to 25%), but fermentation and germination, two processes traditionally undertaken in millet-consuming areas of the world, showed increases of 38.9 and 23.2%, respectively, compared to unprocessed controls<sup>38</sup>. Amongst all the millets, finger millet dietary fibre structure and chemistry is experimentally the most well-elucidated<sup>21</sup> and, hence, provides strong foundations for the computational models aimed at understanding these chemical interactions between key nutrient cations and the arabinoxylan structure of millet grains. Three variations of the arabinoxylan model were constructed, based on a proposed structure of the arabinoxylans found in finger millet<sup>21</sup>. In these models, the main linear chain comprises xylose sugars with mono or di-substituted arabinose and glucuronic acid residues. DFT was used to obtain geometrically optimised structures of cation interactions with the arabinoxylan molecules, and the thermodynamic stability of the resulting complexes was calculated. The chosen cations were potassium (K<sup>+</sup>), calcium (Ca<sup>2+</sup>) and zinc (Zn<sup>2+</sup>). Potassium and calcium ions were chosen due to their high concentrations in the finger millet grains<sup>43</sup>, while zinc was targeted due to both its high concentration amongst the millet species<sup>9</sup> and its prominence in biofortification studies of millet grains<sup>44</sup>.

## Results

### Molecular models

A likely structure of arabinoxylans in finger millet was proposed by Subba Rao & Muralikrishna<sup>21</sup> following the isolation of purified arabinoxylans from finger millet through a series of methods—methylation, <sup>13</sup>C NMR, <sup>1</sup>H NMR, FTIR, GLC-MS, oligosaccharide analysis, periodate oxidation and Smith degradation. They revealed that the backbone of the structure was a β-D (1-4)-xylan, with arabinose residues being both mono- and di-substituted at the C3 and C2 positions of the xylose sugar rings. Additionally, the study indicated that the majority of arabinose substitutions were mono substitutions at the C3 position, while the prominence of doubly substituted arabinose was low<sup>21</sup>. The presence of uronic acid residues, found to be glucuronic acid substituted at the C2 position of the xylose rings, was also detected.

Three simplified variations of the models proposed by Subba Rao & Muralikrishna<sup>21</sup> were created using *CrystalMaker*<sup>®45</sup> as seen in Fig. 1a–c. Geometry optimisation using CASTEP<sup>29</sup> followed, to create highly accurate representations of the arabinoxylan structures. The first model (Fig. 1a) featured the xylan backbone with an arabinose residue substituted at the C3 position of the xylose ring. The second model (Fig. 1b) featured the xylan backbone with both an arabinose residue and a glucuronic acid residue substituted at the C3 and C2 positions of the xylose rings, respectively. The final model (Fig. 1c) featured the xylan backbone with two glucuronic acid residues substituted at the C2 positions of the xylose rings. From here on, these structures will be referred to as PolyXA (Fig. 1a), PolyXGA (Fig. 1b) and PolyXGG (Fig. 1c).

All systems were optimised in a fully charge-saturated state. To this end, glucuronic carboxylic acid groups were deprotonated, as were hydroxyl groups if required. For the PolyXA system, hydroxyl ions on the arabinose and xylan backbone were deprotonated, while for the PolyXGA systems, hydroxyl hydrogen atoms were removed solely for the +2 cations (Ca<sup>2+</sup>, Mg<sup>2+</sup>). However, it should be noted that these OH groups are unlikely to be deprotonated either in the growing millet or within the gastrointestinal tract. By contrast, with a pKa of 2.93<sup>28</sup>, the glucuronic carboxylic acid groups are expected to be fully deprotonated under the same conditions. In this respect, the PolyXGG systems represent the most realistic structures for the doubly charged cations, although it should be noted that quantum mechanical calculations rarely return atomic charges that correspond exactly to the assumed electronic model.

### Cation interaction with the PolyXA structure

**Binding sites.** The removal of a hydrogen atom from O2 (Fig. 2) formed an RCO<sup>-</sup> group, which proved to be a stable binding position for both the

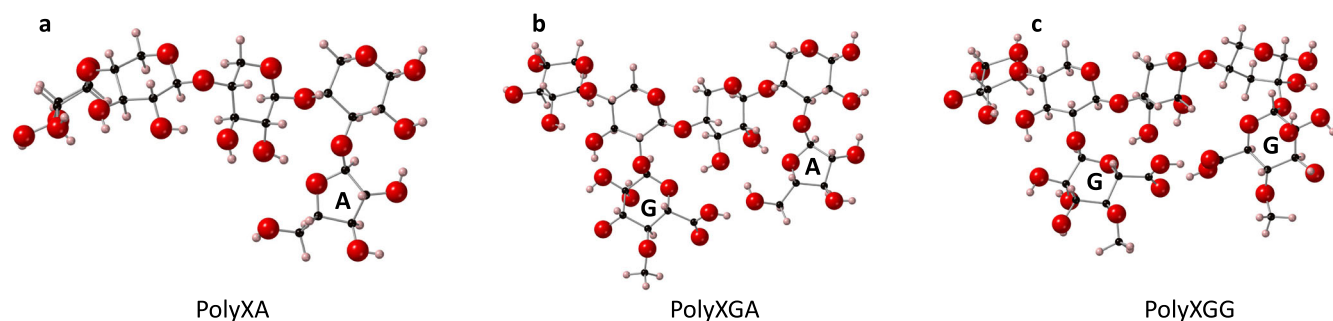


**Fig. 1 | The arabinoxylan models.** **a** PolyXA arabinoxylan consisting of the xylan backbone with one arabinose residue. **b** PolyXGA arabinoxylan consisting of the xylan backbone with one arabinose and one glucuronic acid residue. **c** PolyXGG arabinoxylan consisting of the xylan backbone and two glucuronic acid residues. Carbon atoms are shown in black, hydrogen in pink and oxygen in red. Residues (arabinose (A) and glucuronic acid (G)) are also labelled.

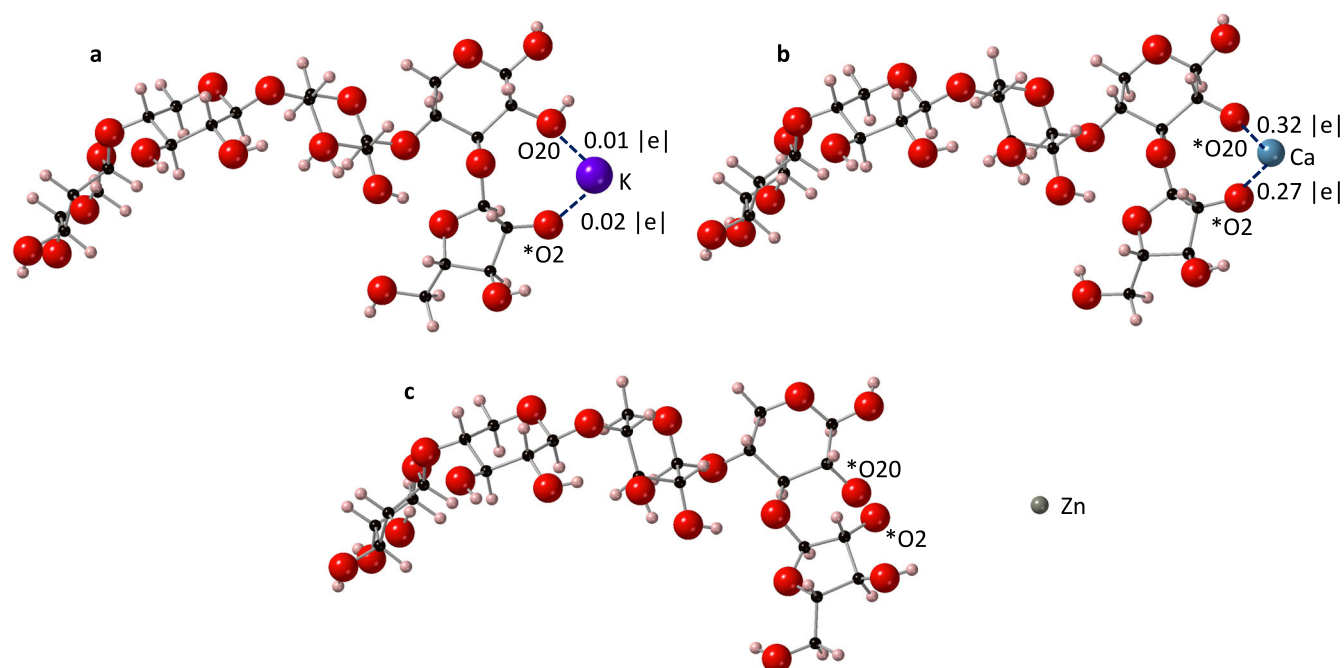


**Fig. 2 | Optimised PolyXA structures with three different cations.** **a**  $K^+$ , **b**  $Ca^{2+}$  and **c**  $Zn^{2+}$ . Ionic bonds to the cations are shown with dotted lines and populations are marked. Atoms with a formal charge are marked with an asterisk (\*). Calcium is shown in blue, potassium in purple, zinc in grey, oxygen in red, carbon in black and hydrogen in pink.

$K^+$  and  $Ca^{2+}$  ions following geometry optimisation (Fig. 2a, b). In the  $K^+$  PolyXA complex, the  $K^+$  ion also formed a bond with the hydroxyl group of the xylan backbone (Fig. 2a), while the  $Ca^{2+}$  ion formed a second ionic bond to the deprotonated OH group of the xylan backbone (Fig. 2b). The observations of the preferential binding positions for  $K^+$  and  $Ca^{2+}$  ions were coherent with other studies. Sharma et al.<sup>46</sup> analysed the interaction of mono and divalent metal ions with fructose using DFT, and revealed that hydroxyl groups acted as the preferred binding sites for the metal ions. A review on calcium-carbohydrate complexes also showed the ability of calcium ions to bind to multiple oxygen atoms within a polysaccharide complex<sup>47</sup>. From Fig. 2c, it is clear that  $Zn^{2+}$  ions do not bind to the PolyXA structure. This result differs from previous work by Sharma et al.<sup>46</sup>, who revealed that zinc was capable of binding to hydroxyl groups of other sugar molecules such as  $\alpha$ -fructose and  $\beta$ -fructose.

### Bond architecture

The coordination number (CN) for both  $K^+$  and  $Ca^{2+}$  ions was found to be 2 (CN = 2), both bonds being to oxygen atoms. This is expected given that there are no other accessible oxygen atoms surrounding the potassium and

calcium ions besides O20 and O2 (Fig. 2). This result aligns well with the work of Sharma et al.<sup>46</sup> who showed that both potassium and calcium ions were bi-coordinated to two hydroxyl groups of  $\alpha$ -fructose and  $\beta$ -fructose, in a coordination geometry that is similar to those of Fig. 2a, b.

Shannon & Prewitt<sup>48</sup> provided a set of effective ionic radii that serve to study bond lengths between cations and oxygen. For the ions considered in this study, the ionic radii trend follows  $K^+(1.38 \text{ \AA}) > Ca^{2+}(1.00 \text{ \AA}) > Zn^{2+}(0.60 \text{ \AA})$ . Here, the average bond length of the  $K^+$ -oxygen bond is 2.505  $\text{\AA}$ , which is greater than the average bond length of the  $Ca^{2+}$ -oxygen bond (2.024  $\text{\AA}$ ), following the trend in ionic radii. Tehrani et al.<sup>49</sup> revealed that when potassium was involved in a bidentate bond with oxygen in sugar molecules, bond lengths ranged from 2.45 to 2.69  $\text{\AA}$ , a result that is representative of the present study.

The bond length between  $K^+$ -O2 (2.298  $\text{\AA}$ ) is shorter than the bond length between  $K^+$ -O20 (2.711  $\text{\AA}$ ), which is to be expected given the formal charge of O2 and its increased electronegativity. The bond lengths of  $Ca^{2+}$ -O2 (2.045  $\text{\AA}$ ) and  $Ca^{2+}$ -O20 (2.003  $\text{\AA}$ ) are comparable, which is also expected given that the calcium ion was bonded to the same RCO functionality.

Mulliken bond populations (Fig. 2) suggest that all cation-oxygen bonds are ionic, as defined by cation-oxygen bond populations  $<0.4 |e|$ . The weak bond populations of the  $K^+$ -O bonds ( $0.01 |e|$  and  $0.02 |e|$ ), are considerably smaller than the average bond population of  $Ca^{2+}$ -O ( $0.30 |e|$ ). This can be explained by the greater charge density of  $Ca^{2+}$  compared to  $K^+$ , resulting in considerably stronger electrostatic forces of attraction with the oxygen atom.

### Thermodynamic stability

The thermodynamic stabilities of the resulting complexes were determined by calculating the formation energy (Eq. 1, Table 1). It is evident that calcium ( $E_f = -1.06$  eV) formed the most stable structures with PolyXA, followed by potassium ( $E_f = -0.19$  eV). The zinc complex, however, remained thermodynamically unfavourable ( $E_f = 4.85$  eV). Given that the charge density trend follows the order of  $Zn^{2+} > Ca^{2+} > K^+$ , it is evident that the stability of the resulting cation-arabinoxylan complex is not solely due to charge density factors. Debon & Tester<sup>50</sup> noted that zinc ions have no affinity for

**Table 1 | Formation energies (eV) for the cation-PolyXA, PolyXGA and PolyXGG complexes**

Structure	$E_f$ (eV)		
	$K^+$	$Ca^{2+}$	$Zn^{2+}$
PolyXA	-0.19	-1.06	4.85
PolyXGA	-1.49	-2.96	0.62
PolyXGG	-3.82	-2.99	4.82

neutral polysaccharides. However, the removal of hydrogen atoms from the O2 and O20 atoms presented two  $RCO^-$  groups that might have been expected to bind to the positive zinc ion if charge density alone were the driver for chemical bonding. Therefore, it is necessary to consider other factors such as effective ionic radius, that can have an effect in determining the stability of the resulting cation-arabinoxylan complex. This will be discussed further in the following sections.

### Cation interaction with the PolyXGA structure

**Binding sites.** In the PolyXGA structure, the removal of hydrogen atoms from O28 and O4 created adjacent  $RCOO^-$  and  $RCO^-$  groups, which provided a stable binding pocket for both the  $Ca^{2+}$  and  $Zn^{2+}$  ions (Fig. 3b, c). In the  $K^+$  PolyXGA complex, the  $RCOO^-$  group provides the stable binding site (Fig. 3a), with the only bond to  $K^+$  formed in this group. It should be noted that the deprotonation of the  $RCOOH$  group of glucuronic acid results in charge resonance effects upon optimisation, such that both oxygen atoms in this group have almost equal charge. These observations corroborate the DFT work of Hills et al.<sup>51</sup> who revealed that the  $RCOO^-$  and hydroxyl groups were favourable binding positions for mono and divalent metal ions ( $Na^+$ ,  $Ca^{2+}$ ,  $Mg^{2+}$ ) within bacterial alginate (mannuronate-guluronate) extracellular matrix complexes. Furthermore, Agulhon et al.<sup>30</sup> demonstrated, also through a DFT study, that transition metals bonded to the hydroxyl or  $RCOO^-$  groups in metal-diuronate complexes.

### Bond architecture

Bond populations and lengths are shown in Supplementary Table 1.  $K^+$  was bonded to just one oxygen atom in the PolyXGA complex (CN = 1), making

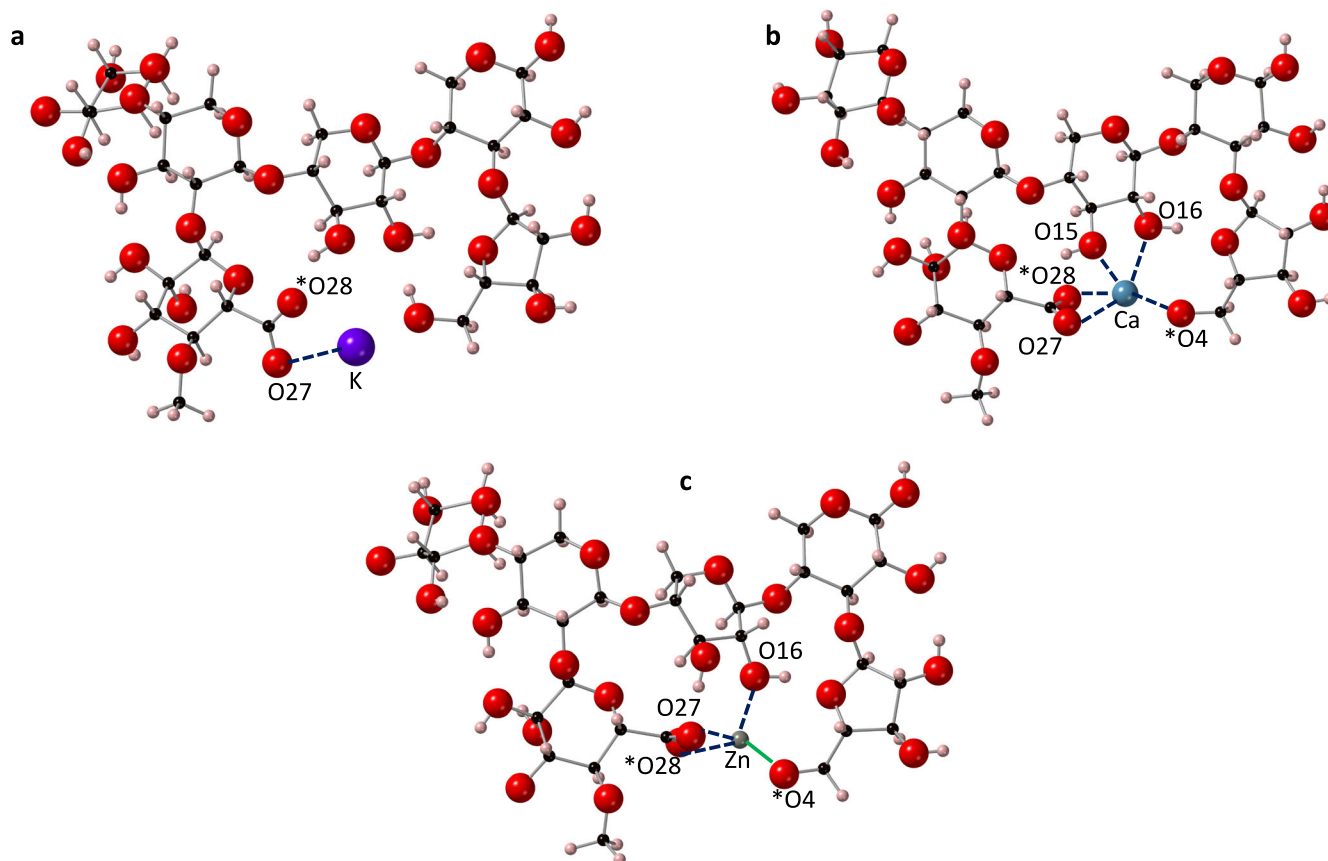


**Fig. 3 | Optimised PolyXGA structures with three different cations. a  $K^+$ , b  $Ca^{2+}$  and c  $Zn^{2+}$ .** Ionic bonds to the cations are shown with dotted lines and the one covalent bond from  $Zn^{2+}$  to O4 is shown as a solid green line. Atoms with a formal charge are marked with an asterisk (\*). Note that due to resonance effects, the formal

charge has become equally split between O27 and O28 upon optimisation. Bond lengths and populations are provided in Table 2. Calcium is shown in blue, potassium in purple, zinc in grey, oxygen in red, carbon in black and hydrogen in pink.

this the lowest CN when compared to  $\text{Ca}^{2+}$  (CN = 5) and  $\text{Zn}^{2+}$  (CN = 4). While the  $\text{Zn}^{2+}$  ion has a greater charge density than the  $\text{Ca}^{2+}$  ion, the difference in CN between the two cations can be explained by their respective sizes (ionic radii of  $\text{Ca}^{2+} > \text{Zn}^{2+}$ ), whereby larger cations are able to form more bonds within complexes<sup>52</sup>. Hills et al.<sup>51</sup> also noted that alkaline earth ions were capable of forming five or six bonds with oxygen atoms of hydroxyl and carboxylate groups in other (alginate) polysaccharides, a result that was mirrored in the present study.

The bond length of the  $\text{K}^+$ -oxygen bond was 2.634 Å, which is greater than the average bond length of the  $\text{Ca}^{2+}$ -oxygen bonds (2.364 Å) and  $\text{Zn}^{2+}$ -oxygen bonds (2.040 Å). The differences in bond lengths can be explained by charge density where  $\text{Zn}^{2+} > \text{Ca}^{2+} > \text{K}^+$ , and a greater charge density would result in stronger electrostatic forces of attraction with the oxygen atom, and hence, a shorter bond length<sup>49</sup>. Agulhon et al.<sup>30</sup> reported DFT-calculated average bond lengths of  $\text{Ca}^{2+}$  to oxygen of around 2.4 Å, which are very similar to the results presented here. Earlier, using X-ray diffraction, Bugg<sup>53</sup> reported that the bond lengths of calcium to oxygen were between 2.38 to 2.54 Å in a calcium-lactose complex. Moving to the zinc-oxygen bonds, in two alternative saccharide monomer complexes ( $\alpha$ -fructose and  $\beta$ -fructose), calculated using DFT,  $\text{Zn}^{2+}$ -oxygen distances were found to be in the region of 2.0 Å. These previous results correspond well with the results presented here.

In the PolyXGA-calcium system, the bond length of  $\text{Ca}^{2+}$ -O28 (2.384 Å) was similar to that of  $\text{Ca}^{2+}$ -O27 (2.355 Å), despite O28 being the formally charged atom. This can be explained by resonance effects at the  $\text{RCOO}^-$  group, where the delocalisation of electrons has resulted in the negative charge being shared between the O28 and O27 atoms. The bond lengths of the  $\text{Ca}^{2+}$ - $\text{RCOO}^-$  bonds were, however, greater than the bond length between  $\text{Ca}^{2+}$ -O4 (2.056 Å). This suggests that the interaction between  $\text{Ca}^{2+}$  and the  $\text{RCO}^-$  functionality of the arabinose residue was stronger than the  $\text{RCOO}^-$  functionality of the glucuronic acid residue. The favouring of the monodentate ( $\text{RCO}^-$  group) over the bidentate ( $\text{RCOO}^-$ ) bond was also seen with  $\text{Zn}^{2+}$ , where the shortest bond length between  $\text{Zn}^{2+}$  and oxygen was between  $\text{Zn}^{2+}$  and O4 (1.82 Å). Once again, this suggests that the  $\text{RCO}^-$  functionality interacted most strongly with the cations. By contrast, Hills et al.<sup>51</sup> noted that the cation and  $\text{RCOO}^-$  interactions in models of *Pseudomonas aeruginosa* bacterial alginate were the strongest and formed the shortest bonds compared to other oxygen groups. However, it should be noted that at physiological pH, the arabinose  $\text{RCOH}$  group would not be expected to be deprotonated. This is further explored in the PolyXGG section below.

Mulliken bond populations (Supplementary Table 1) suggest that all cation-oxygen bonds are ionic, except for the  $\text{Zn}^{2+}$ -O4 bond (0.49 |e|). The ability of zinc to form covalent bonds with oxygen was also highlighted by Agulhon et al.<sup>30</sup>, who showed that both zinc and a number of transition metals, were able to form covalent bonds with oxygen in cation-sugar complexes. The bond population of the  $\text{K}^+$ -O bond (0.01 |e|) is much weaker than the average bond population of both the  $\text{Ca}^{2+}$ -O bonds (0.12 |e|) and the  $\text{Zn}^{2+}$ -O (0.22 |e|) bonds, due to the greater charge densities of  $\text{Zn}^{2+}$  and  $\text{Ca}^{2+}$ .

### Thermodynamic stability

The thermodynamic stabilities of the resulting complexes (Table 1) were determined by calculating the formation energy (Eq. 1). It is evident that  $\text{Ca}^{2+}$  ions ( $E_f = -2.96$  eV) formed the most stable structures with PolyXGA followed by  $\text{K}^+$  ( $E_f = -1.49$  eV), which is also thermodynamically stable, and  $\text{Zn}^{2+}$  ( $E_f = 0.62$  eV), which is unfavourable. A study by Hills et al.<sup>51</sup> also revealed that  $\text{Ca}^{2+}$ , compared to other mono ( $\text{Na}^+$ ) and divalent ( $\text{Mg}^{2+}$ ) cations, formed the most stable complexes amongst bacterial alginates. Given that the charge density of  $\text{Zn}^{2+}$  ions is greater than both potassium and calcium ions, one would expect  $\text{Zn}^{2+}$  to have formed the most stable complexes. Therefore, it is evident that the stability of the resulting cation-arabinosyl complex is not solely due to charge density factors. Steric factors appear to play a much greater role; due to their smaller size, zinc ions have to get closer to other atoms or groups to be within the bond-forming

range, which limits the number of bonds that can be formed. Therefore, it is likely that the zinc ions have to induce greater torsional changes in the PolyXGA structure to create stable chelation sites for binding, which results in an unstable complex.

### Cation interaction with the PolyXGG structure

**Binding sites.** The deprotonation of O24 and O31 atoms created two adjacent  $\text{RCOO}^-$  groups, which formed a stable binding position for both the potassium and calcium ions (Fig. 4a, b). For charge balance, two potassium ions were included in this simulation. In the potassium PolyXGG complex, the  $\text{RCOO}^-$  and hydroxyl groups provided a stable binding position for the K1 ion, while the K2 ion failed to bind despite being situated in a similar environment. As for calcium, the  $\text{RCOO}^-$  groups alone were involved in bonding. Similar observations were noted by DeLucas et al.<sup>54</sup> where, using X-ray diffraction, the carboxyl and hydroxyl groups of glucuronate residues were bonded to the calcium ions. Hills et al.<sup>51</sup> also demonstrated that cations were capable of forming bonds to two  $\text{RCOO}^-$  groups in a cross-linked alginate complex. Additionally, Saladini et al.<sup>55</sup> stated that in sugar acids, the oxygen from both the carboxylic and hydroxyl functionality were involved in the binding of cations. The observations from previous studies align well with the data of the present study.

From Fig. 4c, it is clear that  $\text{Zn}^{2+}$  does not bind to the PolyXGG structure. However, Saladini et al.<sup>55</sup> showed that zinc ion was capable of forming complexes with other sugar acids such as galactaric acid and D-alonic acid.

### Bond architecture

In the  $\text{K}^+$  PolyXGG complex, the CN for K1 is 4, while for K2, the CN is zero, with no bonds formed (Supplementary Table 2). This lack of binding to K2 is likely to be due to repulsive forces between the two potassium ions, preventing co-localisation within the binding pocket. It should be noted, however, that the bond populations are small for the K1-oxygen bonds, and even a minor deviation from an ideal position, results in non-bonding. The CN for the  $\text{Ca}^{2+}$  complex is also 4, but the bonding varies considerably between the two structures. In the  $\text{K}^+$  complex, the one bonding ion forms very weak ionic bonds (0.02 |e|) to one oxygen atom (O23, O30) of each of the deprotonated  $\text{RCOOH}$  groups on the adjacent glucuronic acid residues. Notably, although it was O24 and O31 that were the formally deprotonated oxygen atoms, following optimisation, and through the establishment of resonance effects, it is O23 and O30 that have the greater negative charge,  $-0.73$  e (O23) compared to  $-0.67$  e (O24), and  $-0.74$  e (O30) compared to  $-0.69$  e (O31). In addition, there are two slightly stronger hydrogen bonds from K1 to a ring oxygen (O25) and a hydroxyl oxygen (O27). Similarly, Tian et al.<sup>56</sup> noted that, using FTIR, only one oxygen atom from each  $\text{RCOO}^-$  group was involved in the bonding of  $\text{K}^+$  ions in a  $\text{K}^+$ -galactarate complex. It is also evident that in this complex, the cation- $\text{RCOO}^-$  bonds are now shorter and stronger (in contrast to the PolyXGA system), which corresponds more closely to the results of Hills et al.<sup>51</sup> who made the same observation in binding pockets composed of at least two carboxylic acid residues. In contrast to the  $\text{K}^+$  ions, the  $\text{Ca}^{2+}$  ion sits squarely in the binding pocket between the two adjacent  $\text{RCOO}^-$  groups, bonding to all four oxygen atoms.

The bond lengths between the calcium ion and oxygen atoms were all within 0.12 Å of each other. This suggests that the interactions between  $\text{Ca}^{2+}$  ions and the oxygen atoms of the carboxylic functionality of the glucuronic acid residues were similar in strength. This result can once again be explained by the stabilisation of the  $\text{RCOO}^-$  functionality due to positive steric effects with respect to the size of both the binding pocket and the  $\text{Ca}^{2+}$  ion. With regards to the  $\text{K}^+$  ions, it is interesting to note that although no bonding is predicted to K2 (using Mulliken population analysis), it is nevertheless residing in the vicinity of the second  $\text{RCOO}^-$  group, as illustrated in Fig. 5. It seems likely that the energetics of this position are very similar to that of K1, and the formation energy for the complex overall ( $-3.82$  eV) does indeed suggest favourable binding positions for both ions.

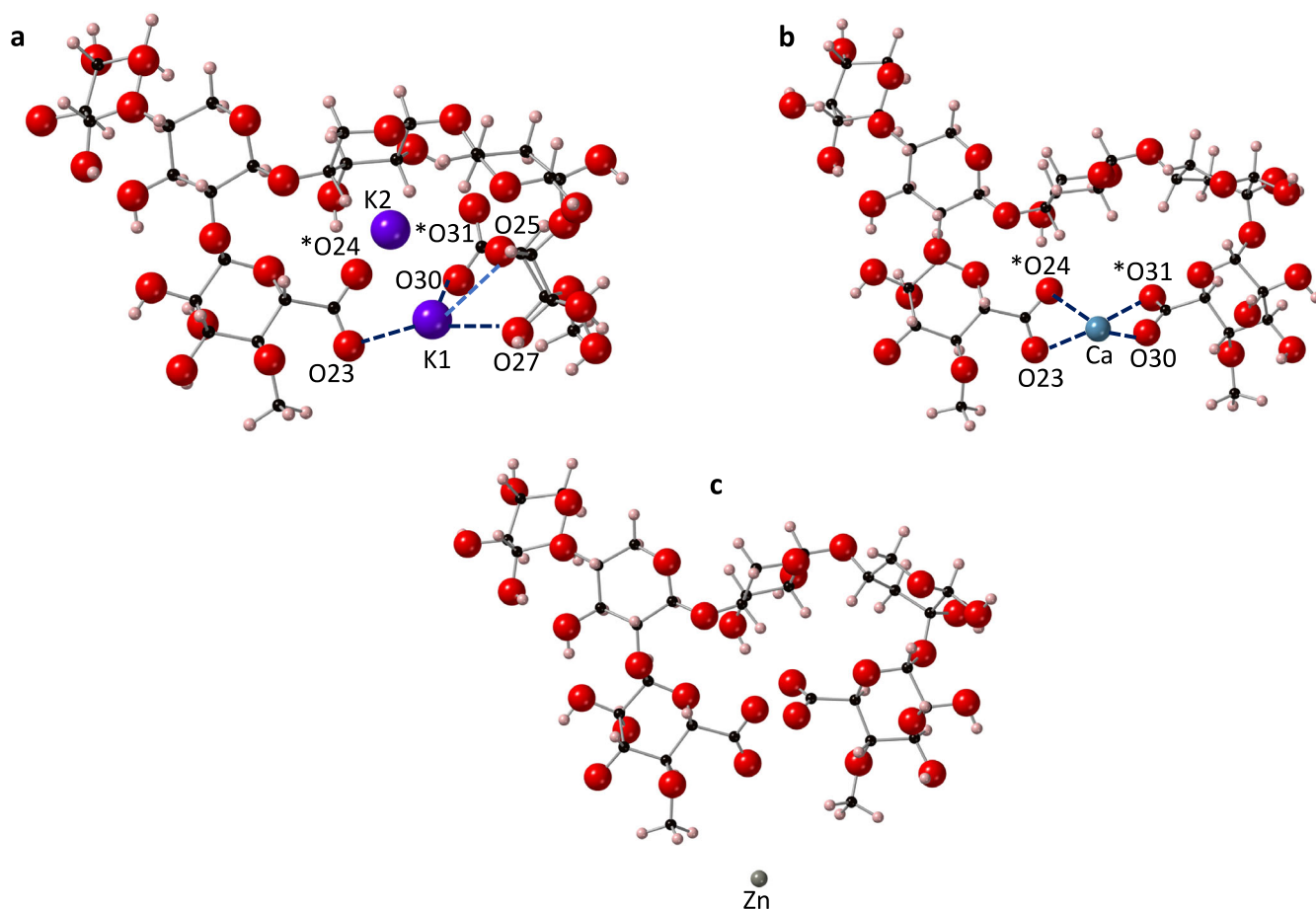


**Fig. 4 | Optimised PolyXGG structures with three different cations. a**  $K^+$ , **b**  $Ca^{2+}$  and **c**  $Zn^{2+}$ . Ionic bonds to the cations are shown with dotted lines. Atoms with a formal charge are marked with an asterisk (\*). Note that due to resonance effects, upon optimisation, the formal charge has become equally split between O23 and

O24, and O30 and O31. Bond lengths and populations are provided in Supplementary Table 2. Calcium is shown in blue, potassium in purple, zinc in grey, oxygen in red, carbon in black and hydrogen in pink.

It should also be noted that with the two glucuronic acid residues, the  $K^+$  now forms its strongest (and shortest) bonds (see Supplementary Table 2).

Mulliken bond populations suggest that all cation-oxygen bonds are ionic. The average bond population of  $K^+$ -O is 0.04 |e|, which is significantly smaller than the average bond population of the  $Ca^{2+}$ -O bonds (0.08 |e|). This is expected given that the charge density of  $Ca^{2+}$  is greater than  $K^+$ , resulting in stronger electrostatic forces of attraction with calcium ions. However, in bacterial alginates (mannuronate/guluronate polysaccharides) average  $Ca^{2+}$ -oxygen bond populations as high as 0.14 |e| have been observed<sup>51</sup>. These higher bond populations were found in binding sites that encompassed not just carboxylic acid groups, but a wider range of oxygen functionality, including hydroxyl and ring oxygen atoms<sup>51</sup>.

### Thermodynamic stability

From Table 1, it is clear that both potassium (−3.82 eV) and calcium (−2.99 eV) formed thermodynamically stable structures with the PolyXGG motif. This is in contrast to zinc (4.82 eV), which proved highly unstable. Given that the charge density trend follows  $Zn^{2+} > Ca^{2+} > K^+$ , it might have been expected that zinc would form the most stable complex within the PolyXGG complex. Indeed, Gianguzza et al.<sup>57</sup> indicated that in glucuronate complexes,  $Zn^{2+}$  formed the most stable complex compared to  $Ca^{2+}$  and  $Na^+$ . Equally, based on charge density arguments alone,  $Ca^{2+}$  ions should have formed more stable complexes with the arabinoxylan structure than potassium ions. However, the lack of stability in zinc binding can be explained using steric factors. Due to its smaller size,  $Zn^{2+}$  ions require a greater torsional change of the PolyXGG backbone structure to create

favourable binding sites.  $K^+$  and  $Ca^{2+}$  clearly have better steric compatibility with the glucuronate-glucuronate binding pockets likely to be found within finger millet.

### Discussion

The interactions between  $K^+$ ,  $Ca^{2+}$  and  $Zn^{2+}$  ions with the xylan backbone (four xylose sugar rings) of the arabinoxylan structure were also calculated (Supplementary Tables 3, 4 and Supplementary Fig. 1). Once again, the results showed that  $Zn^{2+}$  was thermodynamically unfavourable, while both  $Ca^{2+}$  and  $K^+$  ionically bonded to the  $RCO^-$  and hydroxyl groups of the backbone.  $Ca^{2+}$  formed the most stable complex (−0.99 eV), followed by  $K^+$  (−0.42 eV). Initially, the addition of the arabinose residue (PolyXA) improved the stability of the  $Ca^{2+}$ -arabinoxylan complex, but this was not the case for  $Zn^{2+}$ . However, for both  $Ca^{2+}$  and  $K^+$ , the addition of the glucuronic acid residue to the xylan backbone improved the thermodynamic stability of the cation-arabinoxylan complex considerably, as seen in the PolyXGA and PolyXGG structures. The PolyXGG structure, which corresponds most closely to that likely to be found within millet, was able to form the most stable complexes of all with  $Ca^{2+}$  and  $K^+$ .

The inability of  $Zn^{2+}$  to form stable complexes with any of the PolyX structures can be explained by its smaller size, which prevented it from finding a stable multi-oxygen binding pocket across any of the structures. A previous study by Reese et al.<sup>58</sup> looked at the thermodynamic stability of both  $Eu^{3+}$  and  $Cm^{3+}$  with glucuronic acid complexes and found that despite having a smaller charge density, the larger  $Cm^{3+}$  cation was able to form more stable structures than the smaller  $Eu^{3+}$  cation. Furthermore, the

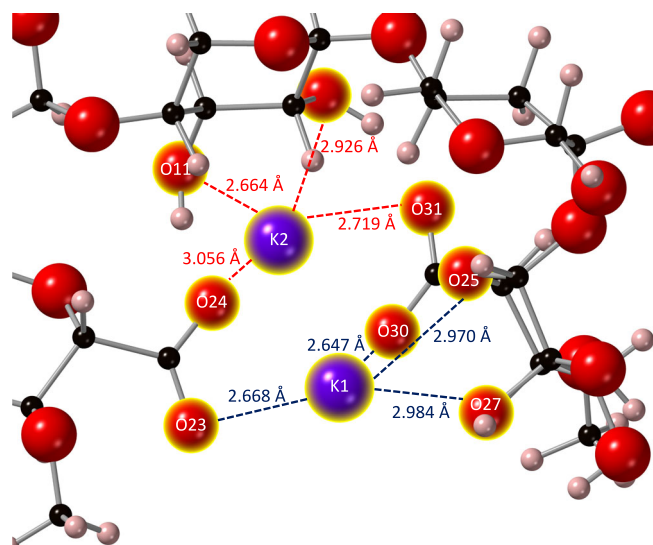


**Fig. 5** | A close-up view of the two  $K^+$  ions in the PolyXGG complex, illustrating the similar binding pocket environments. The Mulliken-predicted bonds to K1 are shown as blue dotted line, and bond distances (not predicted as bonding) to K2 are shown with red dotted lines.

addition of  $Eu^{3+}$  caused a distortion of the glucuronic acid structure, reducing the overall thermodynamic stability of the complex. This phenomenon corresponds well with the results obtained for  $Zn^{2+}$ , which, despite having a higher charge density, showed an inability to bind to the PolyXA and PolyXGG structures. Although  $Zn^{2+}$  was able to bind to the PolyXGA structure, the resulting complex remained thermodynamically unfavourable, suggesting instability of the resulting complex. Hence, it is evident that the ionic radii of the cations play a crucial role in determining the overall stability of cation-sugar complexes where the xylan backbone appears relatively inflexible.

In the present study,  $Ca^{2+}$  formed the most stable complexes in the PolyXA and PolyXGA complexes, while the formation energy of  $K^+$  suggested it formed the most stable PolyXGG complex. Zinc ions were incapable of forming any thermodynamically favourable structures with the arabinoxylan molecule, which suggests that  $Zn^{2+}$  would not bond to this fraction of the finger millet grains. Indeed, these data help to explain the documented nutrient levels of zinc (2.5 mg/100 g), potassium (443 mg/100 g) and calcium (364 mg/100 g) in finger millet, where zinc is present at much lower concentrations<sup>6</sup>. Given the weak binding of zinc in our models, it is unsurprising that measured values are low in fresh, raw grains.

However, free phenolic acids are also present in finger millets<sup>20</sup>, and these compounds could potentially form favourable interactions with zinc and other ions, although to date, no published data have been reported on this. Given these results, it might be suggested that zinc may be relevant as a supplemental ion only (where zinc compounds are simply mixed with millet products, e.g. flours). Given that the formation energies for all calcium and potassium PolyX complexes were thermodynamically favourable, both calcium and potassium ions are likely to exist as bound minerals within the arabinoxylan complex. The bioavailability of the minerals bound to dietary fibre is still a point of discussion, considering factors such as structure, solubility and fermentability of fibre in the gut<sup>5</sup>. However, *in vitro* studies examining cooking and processing methods on calcium bioavailability, suggest millet has a value of around 28%<sup>38</sup>, and the two previous human studies on retention suggest around 25% of calcium is retained within the body<sup>36,37</sup>. Although these bioavailability and retention figures are not particularly large, finger millet has an extremely high level of calcium, which means that overall finger millet is a particularly good source of this mineral. Although humans do not produce xylanolytic enzymes, it is well established that gut microbiota produces a vast array of such molecules, which are capable of degrading the xylan backbone and cleaving the side-chain

residues. This suggests that tight ion-binding, as observed here with potassium and calcium, does not necessarily mean that bioavailability is particularly low, as discussed above. Indeed, it is likely that these ions will be released within the gastrointestinal tract to some extent, as the microbiota-produced degradative enzymes breakdown the structures and disrupt, or completely collapse, the ion-binding pockets we have identified. Earlier studies have reported that the more fermentable and less viscous the bound fibre, the greater the tendency for mineral release<sup>59</sup>. Currently, it is known that arabinoxylans *are* metabolised in the colon to yield short-chain fatty acids (SCFAs), which eventually would lower the gut luminal pH, thus aiding in mineral absorption<sup>60</sup>. Furthermore, the fermentation characteristics of arabinoxylans depend strongly on their structural properties. Complex branching patterns in arabinoxylans from wheat and corn have been shown to decrease fermentation rates *in vitro* in the presence of human faecal bacteria<sup>61</sup>, and the degree of fermentation appears to be lower with fibres that contain a large arabinose component or a larger arabinose:xylose ratio<sup>62</sup>. Hence, the bioavailability of bound minerals may greatly depend on molecular weight, degree of substitution, branching pattern and phenolic acid substitution on the arabinoxylan<sup>28</sup>. Therefore, future experimental validation using *in vivo* models and human subjects is important to understand the implication of structural variations of millet fibres on the binding of minerals and its bioavailability, as is the structural and chemical characterisation of the different arabinoxylan molecules found across the main varieties of millet.

For both the calcium and potassium ions, we revealed that the addition of glucuronic acid residues improved the thermodynamic stability of the PolyX-cation structures, and the cation-PolyXGG complex was the most stable structure of all compared. Our results suggest that even though glucuronic acid residues are present in smaller concentrations than arabinose residues<sup>20</sup>, they play a vital role in determining the overall stability of the cation-arabinoxylan complex, and will perhaps be a limiting factor in terms of cation-binding concentrations. In this study, we utilised the proposed arabinoxylan structure in finger millet by Subba Rao & Muralikrishna<sup>21</sup>, which encompasses predominantly arabinose residues over glucuronic acid residues, across the xylan backbone. Given the results presented here, it would therefore be interesting to determine strains of finger millet that have greater concentrations of glucuronic acid residues within the arabinoxylan structure for targeted breeding programmes, but also to assess the *in vivo* digestibility of these branched structures. Puranik et al.<sup>35</sup> highlight the current interest in finger millet for just such biofortification studies, but they note a frustrating lack of progress in this area. This has been due to many factors, including the difficulty in hybridising a self-fertile crop (as finger millet is), and a lack of robust donor germplasms that are known to have high-calcium stability in multiple different environments.

While DFT is a highly accurate method of computing geometrically optimised structures, the limitation of this model is the use of a small, single-chain structure of the arabinoxylan molecule. Within the living millet structure, it is possible that multiple overlapping arabinoxylan structures would exist, which could present more stable chelation sites and display the cross-linking stability of arabinoxylan structures with cations. Furthermore, interactions of other trace elements (e.g. phosphorus, iron and magnesium) with the arabinoxylan structure have yet to be identified. Also, it is important to understand the interaction of dietary fibres with phytate, phenolics and tannins, which may also eventually impact the mineral bio-accessibility in the grain. Nonetheless, the results in the present study serve as an important starting point in understanding the atomic level chemistry in the millet structure, demonstrating that calcium and potassium cations are indeed capable of forming complexes with the arabinoxylan molecule, stabilised by oxygen atoms of the  $RCOO^-$ ,  $RCO^-$  and hydroxyl functionality of the xylan backbone and side-chain residues.

## Methods

### Computational details

All geometry optimisations were carried out using the plane-wave density functional theory (DFT) code, CASTEP<sup>29</sup>. A convergence-tested



box of  $35 \text{ \AA} \times 20 \text{ \AA} \times 15 \text{ \AA}$  was used for all cation-arabinoxylan complexes, and a convergence-tested cut-off energy of 900 eV was employed. A Monkhorst-Pack k-point grid of  $1 \times 1 \times 1$  was used to sample the Brillouin zone<sup>63</sup>. Ultrasoft pseudopotentials<sup>64</sup> were used throughout, along with the generalised gradient approximation of Perdew–Burke–Ernzerhof for the exchange–correlation functional<sup>65</sup>. The energy, force and displacement tolerances for the geometry optimisation calculations were set to  $1 \times 10^{-5} \text{ eV atom}^{-1}$ ,  $0.001 \text{ \AA}$  and  $0.03 \text{ eV \AA}^{-1}$ , respectively. All molecules were created and visualised using *CrystalMaker*<sup>45</sup>. Mulliken<sup>66</sup> bond populations were calculated to determine the nature of bonds in each of the optimised ion-complexation structures with a bond population of  $<0.40 |e|$  identified as an ionic bond, and a population  $>0.40 |e|$  as a covalent bond. Chemical potentials for calcium, potassium and zinc were calculated based on their pure-metal crystalline structures in the lowest energy state configurations, namely face-centred cubic (FCC) for calcium, body-centred cubic (BCC) for potassium, and hexagonal (HCP) for zinc, as previously described<sup>67</sup>. The chemical potential for hydrogen was calculated from a single molecule. All chemical potential calculations were carried out at the same convergence-tested cut-off energy of 900 eV.

Formation energies were calculated using:

$$E_f = E_{\text{final}} - (E_{\text{initial}} + \mu_A^x - y\mu_H) \quad (1)$$

where  $E_{\text{final}}$  represents the energy of the optimised system,  $E_{\text{initial}}$  is the energy of the initial arabinoxylan structure,  $\mu_A^x$  is the chemical potential of cation A with charge x and  $\mu_H$  is the chemical potential of a single hydrogen atom, with y representing the number of hydrogen atoms required to balance charge x.

## Reporting summary

Further information on research design is available in the Nature Research Reporting Summary linked to this article.

## Data availability

Supplementary Information is available for this publication, which contains the most important data. Bond length and bond population data for PolyXGA and PolyXGG structures and, backbone–cation interaction data and figures are provided. The simulation input and output files required to reproduce all these findings are available to download from: Helen Chappell, Apramita Devi, Wei Cong Matthew Yong, Tsair-Fuh Lin (2023): First Principles Modelling of the Ion-Binding Capacity of Finger Millet. [Dataset]. <https://doi.org/10.5518/1358>.

Received: 22 May 2023; Accepted: 30 April 2024;

Published online: 14 May 2024

## References

- Kumssa, D. B. et al. Dietary calcium and zinc deficiency risks are decreasing but remain prevalent. *Sci. Rep.* **5**, 10974 (2015).
- Zimmermann, M. B. & Hurrell, R. F. Nutritional iron deficiency. *Lancet* **370**, 511–520 (2007).
- Osendarp, S. J. M. et al. Large-scale food fortification and biofortification in low- and middle-income countries: a review of programs, trends, challenges, and evidence gaps. *Food Nutr. Bull.* **39**, 315–331 (2018).
- Baye, K., Guyot, J. P. & Mouquet-Rivier, C. The unresolved role of dietary fibers on mineral absorption. *Crit. Rev. Food Sci. Nutr.* **57**, 949–957 (2017).
- Rousseau, S., Kyomugasho, C., Celus, M., Hendrickx, M. E. G. & Grauwet, T. Barriers impairing mineral bioaccessibility and bioavailability in plant-based foods and the perspectives for food processing. *Crit. Rev. Food Sci. Nutr.* **60**, 826–843 (2020).
- FAO. *Unleashing the Potential of Millets – International Year of Millets 2023* (FAO, 2023).
- FAOSTAT. FAOSTAT. License: CC BY-NC-SA 3.0 IGO. <https://www.fao.org/faostat/en/#data/QCL> (2022).
- Debieu, M., Kanfany, G. & Laplaze, L. Pearl millet genome: lessons from a tough crop. *Trends Plant Sci.* **22**, 911–913 (2017).
- Varshney, R. K. et al. Pearl millet genome sequence provides a resource to improve agronomic traits in arid environments. *Nat. Biotechnol.* **35**, 969–976 (2017).
- Kheya, S. A. et al. Millets: the future crops for the tropics – status, challenges and future prospects. *Heliyon* **9**, e22123 (2023).
- Taylor, J. R. N. & Kruger, J. in *Sorghum and Millets: Chemistry, Technology, and Nutritional Attributes* Ch. 7 (Elsevier, 2018).
- Kumar, R. R. et al. Iron and zinc at a cross-road: a trade-off between micronutrients and anti-nutritional factors in pearl millet flour for enhancing the bioavailability. *J. Food Compos. Anal.* **111**, 104591 (2022).
- Bijalwan, V., Ali, U., Kesarwani, A. K., Yadav, K. & Mazumder, K. Hydroxycinnamic acid bound arabinoxylans from millet bran-structural features and antioxidant activity. *Int. J. Biol. Macromol.* **88**, 296–305 (2016).
- Malleshi, N. G., Desikachar, H. S. R. & Tharanathan, R. N. Free sugars and non-starchy polysaccharides of finger millet (*Eleusine coracana*), pearl millet (*Pennisetum typhoideum*), foxtail millet (*Setaria italica*) and their malts. *Food Chem.* **20**, 253–261 (1986).
- Nandini, C. D. & Salimath, P. V. Structural features of arabinoxylans from bajra (pearl millet). *J. Agric. Food Chem.* **50**, 6485–6489 (2002).
- Sharma, S., Saxena, D. C. & Riar, C. S. Characteristics of  $\beta$ -glucan extracted from raw and germinated foxtail (*Setaria italica*) and kodo (*Paspalum scrobiculatum*) millets. *Int. J. Biol. Macromol.* **118**, 141–148 (2018).
- Palaniappan, A., Yuvaraj, S. S., Sonaimuthu, S. & Antony, U. Characterization of xylan from rice bran and finger millet seed coat for functional food applications. *J. Cereal Sci.* **75**, 296–305 (2017).
- Savitha Prashanth, M. R. & Muralikrishna, G. Arabinoxylan from finger millet (*Eleusine coracana*, v. Indaf 15) bran: purification and characterization. *Carbohydr. Polym.* **99**, 800–807 (2014).
- Subba Rao, M. V. S. S. T. & Muralikrishna, G. Non-starch polysaccharides and bound phenolic acids from native and malted finger millet (Ragi, *Eleusine coracana*, Indaf - 15). *Food Chem.* **72**, 187–192 (2001).
- Subba Rao, M. V. S. S. T. & Muralikrishna, G. Evaluation of the antioxidant properties of free and bound phenolic acids from native and malted finger millet (ragi, *Eleusine coracana* Indaf-15). *J. Agric. Food Chem.* **50**, 889–892 (2002).
- Subba Rao, M. V. S. S. T. & Muralikrishna, G. Structural analysis of arabinoxylans isolated from native and malted finger millet (*Eleusine coracana*, ragi). *Carbohydr. Res.* **339**, 2457–2463 (2004).
- Subba Rao, M. V. S. S. T. & Muralikrishna, G. Hemicelluloses of ragi (Finger millet, *Eleusine coracana*, indaf-15): Isolation and purification of an alkali-extractable arabinoxylan from native and malted hemicellulose B. *J. Agric. Food Chem.* **54**, 2342–2349 (2006).
- Zhu, Y. et al. Physicochemical and functional properties of dietary fiber from foxtail millet (*Setaria italica*) bran. *J. Cereal Sci.* **79**, 456–461 (2018).
- Maha Lakshmi, R. & Sumathi, S. Binding of iron, calcium and zinc by fibre of sorghum and ragi. *Food Chem.* **60**, 213–217 (1997).
- Amalraj, A. & Pius, A. Influence of oxalate, phytate, tannin, dietary fiber, and cooking on calcium bioavailability of commonly consumed cereals and millets in India. *Cereal Chem. J.* **92**, 389–394 (2015).
- Lestienne, I., Caporiccio, B., Besançon, P., Rochette, I. & Trèche, S. Relative contribution of phytates, fibers, and tannins to low iron and zinc in vitro solubility in pearl millet (*Pennisetum glaucum*) flour and grain fractions. *J. Agric. Food Chem.* **53**, 8342–8348 (2005).
- Chen, Z. et al. Arabinoxylan structural characteristics, interaction with gut microbiota and potential health functions. *J. Funct. Foods* **54**, 536–551 (2019).

28. Wang, J. et al. Cereal-derived arabinoxylans: structural features and structure–activity correlations. *Trends Food Sci. Technol.* **96**, 157–165 (2020).
29. Clark, S. J. et al. First principles methods using CASTEP. *Z. F.ür. Kristallographie - Crystalline Mater.* **220**, 567–570 (2005).
30. Agulhon, P., Markova, V., Robitzer, M., Quignard, F. & Mineva, T. Structure of alginate gels: interaction of diuronate units with divalent cations from density functional calculations. *Biomacromolecules* **13**, 1899–1907 (2012).
31. Bekri, L., Zouaoui-Rabah, M., Springborg, M., & Rahal, M. S. A structural DFT study of MM, GG, MG, and GM alginic acid disaccharides and reactivity of the MG metallic complexes. *J. Mol. Model.* **24**, 312 (2018).
32. Ezzat, H. et al. Dft: B3lyp/ lanl2dz study for the removal of fe, ni, cu, as, cd and pb with chitosan. *Biointerface Res. Appl. Chem.* **10**, 7002–7010 (2020).
33. Plazinski, W. & Drach, M. Calcium- $\alpha$ -l-gulonate complexes: Ca<sup>2+</sup> binding modes from DFT-MD simulations. *J. Phys. Chem. B* **117**, 12105–12112 (2013).
34. Plazinski, W. & Drach, M. Binding of bivalent metal cations by  $\alpha$ -l-gulonate: insights from the DFT-MD simulations. *N. J. Chem.* **39**, 3987–3994 (2015).
35. Puranik, S. et al. Harnessing finger millet to combat calcium deficiency in humans: challenges and prospects. *Front. Plant Sci.* **8**, 1311 (2017).
36. Joseph, K., Kurien, P. P., Swaminathan, M. & Subramaniyan, V. The effect of partial or complete replacement of rice in poor vegetarian diets by ragi (*Eleusine coracana*) on the metabolism of nitrogen, calcium and phosphorus. *Br. J. Nutr.* **12**, 213–218 (1958).
37. Kurien, P. P. & Dorauswamy, T. R. Effect of replacing cereal in a poor diet with whole or refined ragi flour on the nutritional status and metabolism of nitrogen, calcium and phosphorus in children (boys). *J. Nutr. Dietetics* **4**, 102–109 (1967).
38. Anitha, S. et al. Calcium from finger millet – a systematic review and meta-analysis on calcium retention, bone absorption, and in vitro bioavailability. *Sustainability* **13**, 8677 (2021).
39. Mamiro, P. R. S., Van Camp, J., Mwikya, S. M. & Huyghebaert, A. In vitro extractability of calcium, iron and zinc in finger millet and kidney beans during processing. *Food Chem. Toxicol.* **66**, 1271–1275 (2001).
40. Krishnan, R., Dharmaraj, U. & Malleshi, N. G. Influence of decortication, popping and malting on bioaccessibility of calcium, iron, and zinc in finger millet. *Food Sci. Technol.* **48**, 169–174 (2012).
41. Sriprya, G., Antony, U. & Chandra, T. S. Changes in carbohydrate, free amino acids, organic acids, phytate and HCl extractability of minerals during germination and fermentation of finger millet (*Eleusine coracana*). *Food Chem.* **58**, 345–350 (1997).
42. Platel, K., Epieson, S. W. & Srinivasan, K. Bioaccessible mineral content of malted finger millet (*Eleusine coracana*), wheat (*Triticum aestivum*), and Barley (*Hordeum vulgare*). *J. Agric. Food Chem.* **58**, 8100–8103 (2010).
43. Jayawardana, S. A. S. et al. Dietary fibers, starch fractions and nutritional composition of finger millet varieties cultivated in Sri Lanka. *J. Food Compos. Anal.* **82**, 103249 (2019).
44. Kodkany, B. S. et al. Biofortification of pearl millet with iron and zinc in a randomized controlled trial increases absorption of these minerals above physiologic requirements in young children. *J. Nutr.* **143**, 1489–1493 (2013).
45. CrystalMaker. CrystalMaker®: a crystal and molecular structures program for Mac and Windows. CrystalMaker Software Ltd. [www.crystallmaker.com](http://www.crystallmaker.com) (2022).
46. Sharma, D., Kanchi, S., Bathinapatla, A., Inamuddin & Asiri, A. M. Modeling of neotame and fructose thermochemistry: comparison with mono and divalent metal ions by computational and experimental approach. *Sci. Rep.* **9**, 18414 (2019).
47. Dheu-Andries, M. L. & Pérez, S. Geometrical features of calcium-carbohydrate interactions. *Carbohydr. Res.* **124**, 324–332 (1983).
48. Shannon, R. D. & Prewitt, C. T. Effective ionic radii in oxides and fluorides. *Acta Crystallogr. Sect. B Struct. Crystallogr. Cryst. Chem.* **25**, 925–946 (1969).
49. Tehrani, Z. A., Fattahi, A. & Pourjavadi, A. DFT study of the interaction of cytidine and 2'-deoxycytidine with Li<sup>+</sup>, Na<sup>+</sup>, and K<sup>+</sup>: effects of metal cationization on sugar puckering and stability of the N-glycosidic bond. *Carbohydr. Res.* **344**, 771–778 (2009).
50. Debon, S. J. J. & Tester, R. F. In vitro binding of calcium, iron and zinc by non-starch polysaccharides. *Food Chem.* **73**, 401–410 (2001).
51. Hills, O. J., Smith, J., Scott, A. J., Devine, D. A. & Chappell, H. F. Cation complexation by mucoid *Pseudomonas aeruginosa* extracellular polysaccharide. *PLoS ONE* **16**, e0257026 (2021).
52. Alvarado, L. et al. Supramolecular assemblies prepared from an iron(II) tripodal complex, tetrafluoroborate, and alkali metal cations. the effect of cation size on coordination number, anion disorder and hydrogen bonding. *CrystEngComm* **11**, 2297–2307 (2009).
53. Bugg, C. E. Calcium binding to carbohydrates. Crystal structure of a hydrated calcium bromide complex of lactose. *J. Am. Chem. Soc.* **95**, 908–913 (1973).
54. DeLucas, L., Bugg, C. E., Terzis, A. & Rivest, R. Calcium binding to D-glucuronate residues: crystal structure of a hydrated calcium bromide salt of D-glucuronic acid. *Carbohydr. Res.* **41**, 19–29 (1975).
55. Saladini, M., Menabue, L. & Ferrari, E. Sugar complexes with metal<sup>2+</sup> ions: thermodynamic parameters of associations of Ca<sup>2+</sup>, Mg<sup>2+</sup> and Zn<sup>2+</sup> with galactaric acid. *Carbohydr. Res.* **336**, 55–61 (2001).
56. Tian, W., Yang, L.-M., Xu, Y.-Z., Weng, S.-F. & Wu, J.-G. Sugar interaction with metal ions. FT-IR study on the structure of crystalline galactaric acid and its K<sup>+</sup>, NH<sub>4</sub><sup>+</sup>, Ca<sup>2+</sup>, Ba<sup>2+</sup>, and La<sup>3+</sup> complexes. *Carbohydr. Res.* **324**, 45–52 (2000).
57. Gianguzza, A., Maggio, F. & Sammartano, S. Glucuronate complexes with Mg<sup>2+</sup>, Ca<sup>2+</sup>, Zn<sup>2+</sup> and Cd<sup>2+</sup> in aqueous chloride solution: a possible chemical speciation model for biochemical understanding. *Chem. Speciat. Bioavailab.* **8**, 17–21 (1996).
58. Reese, S., Kaden, P., Taylor, C. J., Kloditz, R. & Schmidt, M. Structure and thermodynamics of Eu(III) and Cm(III) complexes with glucuronic acid. *Inorg. Chem.* **60**, 14667–14678 (2021).
59. Trinidad, T. P., Wolever, T. M. S., & Thompson, L. U. Availability of calcium for absorption in the small intestine and colon from diets containing available and unavailable carbohydrates: an in vitro assessment. *Int. J. Food Sci. Nutr.* (1996) **47**, 83–88
60. Tremaroli, V. & Bäckhed, F. Functional interactions between the gut microbiota and host metabolism. *Nature* **489**, 242–249 (2012).
61. Rumpagaporn, P. Structural features of soluble cereal arabinoxylan fibers associated with a slow rate of in vitro fermentation by human fecal microbiota. *Carbohydr. Polym.* **130**, 191–197 (2015).
62. Pollet, A. et al. In vitro fermentation of arabinoxylan oligosaccharides and low molecular mass arabinoxylans with different structural properties from wheat (*Triticum aestivum* L.) bran and psyllium (*Plantago ovata* Forsk) seed husk. *J. Agric. Food Chem.* **60**, 946–954 (2012).
63. Monkhorst, H. J. & Pack, J. D. Special points for Brillouin-zone integrations. *Phys. Rev. B* **13**, 5188–5192 (1976).
64. Vanderbilt, D. Soft self-consistent pseudopotentials in a generalized eigenvalue formalism. *Phys. Rev. B* **41**, 7892 (1990).
65. Perdew, J. P., Burke, K. & Ernzerhof, M. Generalized gradient approximation made simple. *Phys. Rev. Lett.* **77**, 3865–3868 (1996).
66. Mulliken, R. S. Electronic population analysis on LCAO-MO molecular wave functions. I. *J. Chem. Phys.* **23**, 1833–1840 (1955).
67. Chappell, H. F. & Bristowe, P. D. Density functional calculations of the properties of silicon-substituted hydroxyapatite. *J. Mater. Sci. Mater. Med.* **18**, 829–837 (2007).

## Acknowledgements

This work was undertaken on ARC4, part of the High-Performance Computing facilities at the University of Leeds, UK.

## Author contributions

MY: Methodology, investigation, formal analysis, data curation and writing—original draft and review; AD: Conceptualisation, visualisation, writing—original draft, review, editing and proofreading, funding acquisition; T-FL: Resources, writing—review, editing and proofreading; HC: Conceptualisation, methodology, formal analysis, writing—original draft, review, editing and proofreading, resources and visualisation.

## Competing interests

The authors declare no potential conflicts of interest with respect to the research, authorship, and/or publication.

## Additional information

**Supplementary information** The online version contains supplementary material available at <https://doi.org/10.1038/s41538-024-00270-1>.

**Correspondence** and requests for materials should be addressed to Helen F. Chappell.

**Reprints and permissions information** is available at <http://www.nature.com/reprints>

**Publisher's note** Springer Nature remains neutral with regard to jurisdictional claims in published maps and institutional affiliations.

**Open Access** This article is licensed under a Creative Commons Attribution 4.0 International License, which permits use, sharing, adaptation, distribution and reproduction in any medium or format, as long as you give appropriate credit to the original author(s) and the source, provide a link to the Creative Commons licence, and indicate if changes were made. The images or other third party material in this article are included in the article's Creative Commons licence, unless indicated otherwise in a credit line to the material. If material is not included in the article's Creative Commons licence and your intended use is not permitted by statutory regulation or exceeds the permitted use, you will need to obtain permission directly from the copyright holder. To view a copy of this licence, visit <http://creativecommons.org/licenses/by/4.0/>.

© The Author(s) 2024